03.1

Competition between instability mechanisms of a supersonic overexpanded air jet as it flows into water

© K.N. Volkov, V.N. Emelyanov, M.S. Yakovchuk

Baltic State Technical University, St. Petersburg, Russia
E-mail: dsci@mail.ru

Received August 10, 2023
Revised September 18, 2023
Accepted September 18, 2023

An analysis is made of the structural features of turbulence formed when a supersonic air jet flows into water. At a qualitative level, a comparison is made of the flow pattern when an air jet flows into air and water. The results of numerical simulation of the jet velocity field are used to analyze the Kelvin–Helmholtz and Rayleigh–Taylor instability mechanisms and to identify the dominant mechanism in various jet propagation regions. The results obtained are compared with experimental high-speed photographic recording data and available numerical calculations.

Keywords: underwater outflow, supersonic jet, simulation of large eddies, instability.

DOI: 10.61011/TPL.2023.11.57193.19706

The gas–liquid interaction complicates considerably the processes occurring in outflowing underwater supersonic jets [1,2]. The formation of shock waves and their interaction with the interface alter the shape of the free surface and induce its instability. An increase in the external pressure (i.e., the depth at which an outflowing jet resides) translates into an enhancement of the interaction between gas and liquid and induces instability of their interface [3,4]. The results of experimental studies are indicative of instability of the specific impulse in the context of an underwater supersonic jet and suggest that buoyancy forces exert a considerable influence here [5]. The Kelvin–Helmholtz and Rayleigh–Taylor instabilities have a substantial effect on the formation of the phase interface [6–8].

The use of an axially symmetric formulation of the problem leads to an incorrect flow pattern. RANS (Reynolds-averaged Navier–Stokes) equations do not take into account the pulsations of pressure near the nozzle exit for an outflowing underwater air jet. The mixing layer instability is attributed to the emergence of azimuthal inhomogeneity of large eddies, which results in decay of ring eddies in the end of the initial section [9].

The calculation domain reproduces the geometric dimensions of the experimental setup [7] and has the form of a vertical cylinder 1 m in height and 0.5 m in diameter. The lower base of this cylinder features a cylindrical cavity 26 mm in radius with a submerged ultrasonic nozzle. The diameter of the nozzle throat section is $d_c = 2$ mm, the diameter of the nozzle exit section is $d_e = 2.5$ mm, and the diameter of the nozzle inlet section is $d_i = 16$ mm. The nozzle has a cylindrical part and two conical parts. Its inlet part is formed by a cylinder 20 mm in height and a truncated cone. The exit (expanding) nozzle part is a truncated cone 12 mm in height. The characteristics of the calculation domain and input parameters of the problem were discussed in detail in [9].

The geometric Mach number of the nozzle is 1.9 (the nozzle expansion ratio is 1.5625). A fully expanded flow from the nozzle forms at NPR (nozzle pressure ratio) = 1.7613 ($n = 0.1479$). A fully subsonic outflow from the nozzle (the flow regime with overexpansion) is observed at NPR = 1.1221 ($n = 0.02978$). A closing shock in the nozzle exit section forms at NPR = 1.6756 ($n = 0.5983$).

A full-flow start with a region of elevated pressure specified at the initial time in the cylindrical inlet part of the nozzle is reproduced in calculations. A total pressure of 6.7 MPa is set in the nozzle inlet section (under these conditions, an air jet outflows into air in the design regime, while an underwater air jet is overexpanded). The static pressure corresponding to the given depth and the temperature are fixed at the outer boundaries of the computational domain. The pressure corresponding to the given depth is set as an initial condition.

The shape of the phase interface is characterized using the VOF (volume of fluid) method. The equation of state of an ideal gas is used for air. The compressibility of liquid is taken into account in accordance with the Tait equation of state. The SBES (stress-blended eddy simulation) method, which is a hybrid RANS/LES approach (LES — large eddy simulation) [10], is used for turbulence modeling. The SBES approach has no explicit dependence on the grid resolution, providing fast switching between RANS and LES in the flow separation region. The SST turbulence model is used in RANS calculations, and the WALE (wall-adapting local eddy-viscosity) subgrid model is applied in the LES method. Calculations are performed on a block-structured grid with approximately 10 million cells in an unsteady formulation with a time step of 2 μs. The major equations are integrated up to the time point of 10 ms.

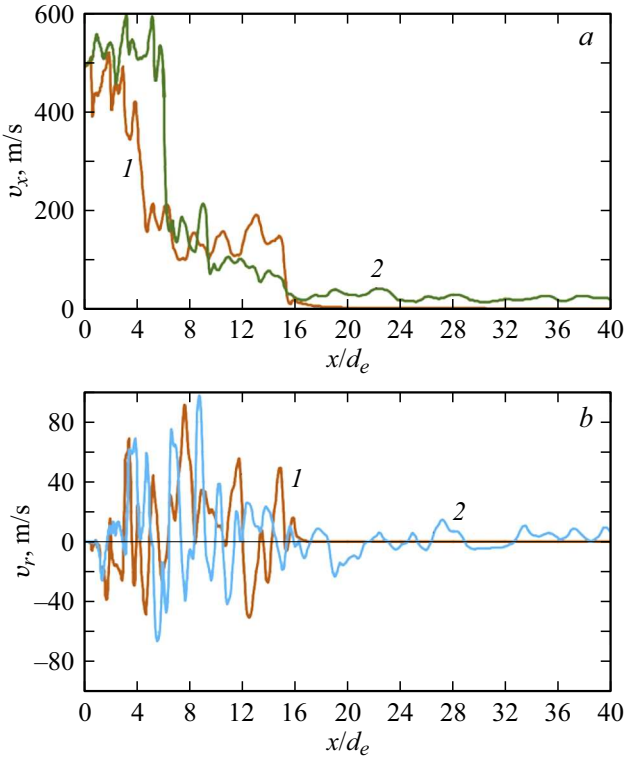

Figure 1. Distributions of axial (*a*) and radial (*b*) velocity component at the jet axis at two time points: 1 (*1*) and 10 ms (*2*).

The Kelvin–Helmholtz instability mechanism is associated with the velocity gradient on the interface surface. The Rayleigh–Taylor instability mechanism is related to the effect of gravity and buoyancy forces. The model proposed in [11] is used to analyze the mechanism of instability of the phase interface of a jet. The contribution of the Rayleigh–Taylor instability is characterized by coefficient

$$C_{\mathrm{RT}} = 2\pi \frac{d_e}{m_e} r(x)\left\{\frac{2}{3}\rho_g[3\sigma\rho_w a(x)]^{1/2}\right\}^{1/2}.$$

The contribution of the Kelvin–Helmholtz instability is characterized by coefficient

$$C_{\mathrm{KG}} = \frac{2\pi}{\sqrt{3}} \frac{d_e}{m_e} \rho_g u(x) r(x).$$

Here, d_e is the diameter of the nozzle exit section, m_e is the mass rate of gas flow through the nozzle, $r(x)$ is the radial distance from the jet symmetry axis to the free surface at distance x from the nozzle exit, ρ_g -is the gas density, ρ_w is the liquid density, σ is the surface tension coefficient, $u(x)$ is the axial velocity of gas at distance x from the nozzle exit, and $a(x)$ is the acceleration of the phase interface at distance x from the nozzle exit.

The relative contribution of each mechanism into the jet instability is characterized by instability coefficient

$$\psi = \left(\frac{C_{\mathrm{RT}}}{C_{\mathrm{KG}}}\right)^4 = \frac{\sigma\rho_w a_{r=R}}{\rho_g^2 u_{r=R}^4}$$

where R is the jet radius. At $\psi \ll 1$, the Kelvin–Helmholtz instability mechanism is dominant, while the Rayleigh–Taylor instability mechanism dominates at $\psi \gg 1$. Unsteady characteristics of a jet (such as the velocity and acceleration of the phase interface) need to be determined in order to calculate the instability coefficient.

An exponential nature of attenuation of the axial jet velocity is presumed in empirical models, which also do not take the influence of variations of the phase interface position on the jet velocity into account [8]. The results of numerical modeling are used to make a conclusion regarding the competition between two instability mechanisms. It is assumed for simplicity that the jet boundary in the steady outflow regime has the shape of a truncated cone with a an angle of 24.62°. In agreement with the data from [7], the jet boundary is approximated fairly closely by line $r = 4.582x - 11.66$ (radial coordinate r is expressed in mm).

The instability coefficient is determined after calculation of the flow field and depends to a considerable extent on the accuracy of obtained distributions of velocity components. The results of comparison between calculated and experimental data were discussed in [9]. The distributions of axial and radial velocity components are taken from the calculated data presented in Figs. 1 and 2. Owing to the pressure difference, a vertical impulse is imparted to air at the initial time, and it starts outflowing from the nozzle and displacing water. A typical jet flow interacting with

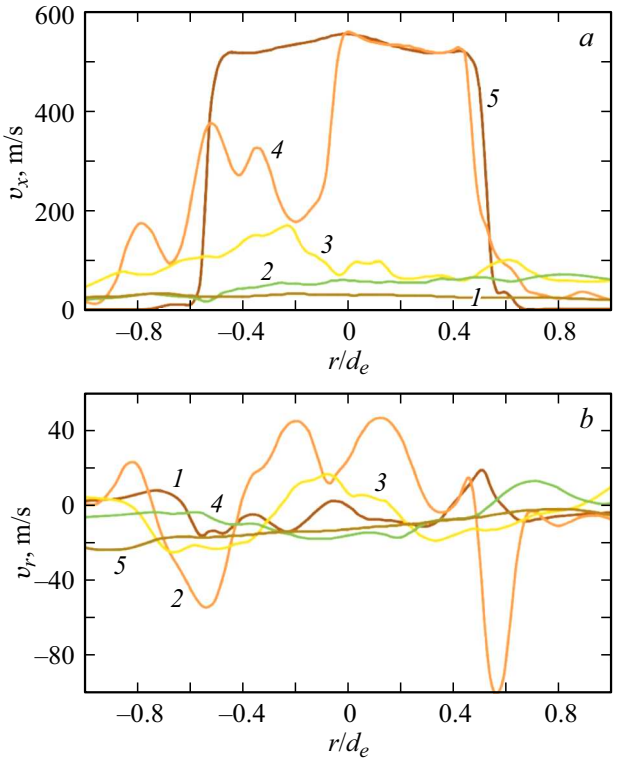

Figure 2. Distributions of axial (*a*) and radial (*b*) velocity component at the jet axis in transverse sections $x/d_e = 1$ (*1*), 5 (*2*), 10 (*3*), 15 (*4*), and 20 (*5*) at the time point of 10 ms.

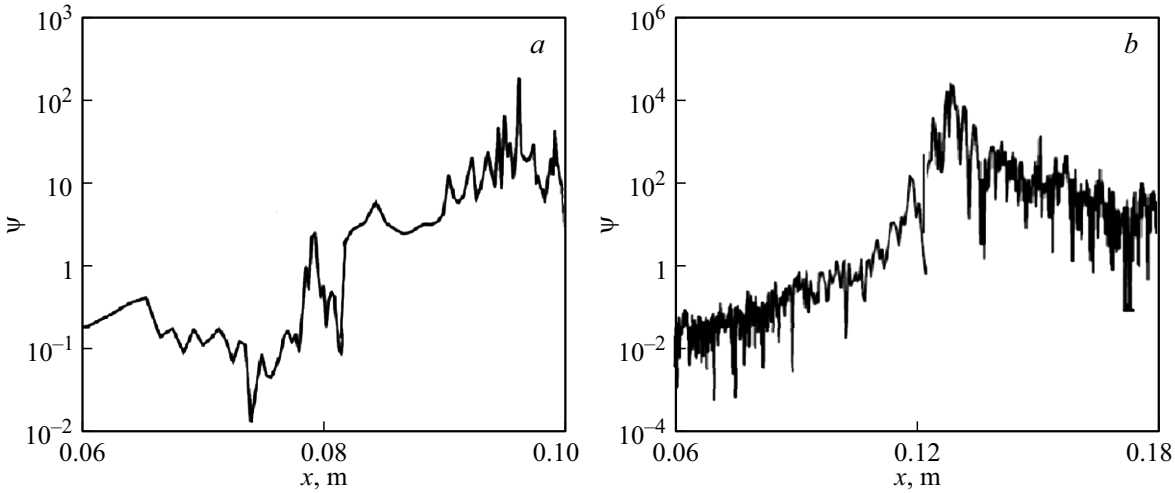

Figure 3. Distributions of the instability coefficient along the jet axis at two time points: 1 (*a*) and 10 ms (*b*).

surrounding water forms. The pressure in water increases as a result of this interaction, thus inducing a reduction in the jet velocity. As gas outflows from the nozzle, air occupies the region near the shear boundary, and the pressure difference decreases. This leads to a reduction in the velocity of air outflow from the nozzle. The vertical velocity of a jet increases in the upward direction. The pressure in surrounding water decreases, and the region occupied by air expands. This is the reason why the jet velocity increases. In addition, the jet velocity near the symmetry axis is higher than the velocity in the jet periphery. The velocity at the jet axis remains fairly high at the initial stage of jet expansion and decreases rapidly afterwards. The velocity at the interface is an order of magnitude lower than the velocity at the jet axis. At a distance on the order of $14d_e$ from the nozzle exit (approximately 0.1 m), the velocity at the jet axis.decreases to 100 m/s.

The acceleration at the interface is determined by processing the results of numerical modeling within the given time interval (10 ms). At the initial stage of jet expansion, the acceleration of the interface is fairly high and increases gradually downstream from the nozzle exit, where the free surface starts to deform. The instability coefficient varies within a fairly wide interval, suggesting that the instability mechanism changes in time and space (Fig. 3). The instability coefficient near the nozzle exit (in the region of high gas velocities) is lower than unity. The Kelvin–Helmholtz instability exerts the dominant influence on a jet in this region. As the axial jet velocity decreases (intermediate range of variation of the governing coefficient), the Kelvin–Helmholtz and Rayleigh–Taylor instability mechanisms become roughly equal in the order of magnitude. The instability coefficient exceeds unity downstream of the nozzle (in the region of low axial gas velocities), indicating that the Rayleigh–Taylor mechanism is dominant.

Funding

This study was supported by a grant from the Russian Science Foundation (project No. 21-19-00657, https://rscf.ru/project/21-19-00657).

Conflict of interest

The authors declare that they have no conflict of interest.

References

[1] S.S. Gulawani, S.S. Deshpande, J.B. Joshi, Ind. Eng. Chem. Res., **46**, 3188 (2007). DOI: 10.1021/ie0608511
[2] S. Cloette, J.E. Olsen, Appl. Ocean Res., **31**, 220 (2009). DOI: 10.1016/j.apor.2009.09.005
[3] L. Zhou, Y. Yu, Ocean Eng., **109**, 410 (2015). DOI: 10.1016/j.oceaneng.2015.09.025
[4] B.J. Olson, S.K. Lele, Phys. Fluids, **25**, 110809 (2013). DOI: 10.1063/1.4819349
[5] S. Han, K.H. Moon, S. Ko, J.K. Kim, H.J. Moon, Y.J. You, M.C. Kwan, in *53rd AIAA/SAE/ASEE Joint Propulsion Conf.* (Atlanta, 2017), AIAA paper 2017-5046. DOI: 10.2514/6.2017-5046
[6] C. Weiland, P.P. Vlachos, Int. J. Multiphase Flow, **48**, 46 (2013). DOI: 10.1016/j.ijmultiphaseflow.2012.08.002
[7] X. Zhang, S. Li, B. Yang, N. Wang, Ocean Eng., **213**, 107611 (2020). DOI: 10.1016/j.oceaneng.2020.107611
[8] X. Zhang, S. Li, S. Yu, B. Yang, N. Wang, Water, **12**, 488 (2020). DOI: 10.3390/w12020488
[9] M.S. Yakovchuk, K.N. Volkov, V.N. Emelyanov, J. Phys.: Conf. Ser., **2388**, 012111 (2022). DOI: 10.1088/1742-6596/2388/1/012111
[10] F. Menter, A. Huppe, A. Matyushenko, D. Kolmogorov, Appl. Sci., **11**, 2459 (2021). DOI: 10.3390/app11062459
[11] M. Epstein, H.K. Fauske, S. Kubo, T. Nakamura, K. Koyama, Nucl. Eng. Des., **210**, 53 (2001). DOI: 10.1016/S0029-5493(01)00436-8

Translated by D.Safin